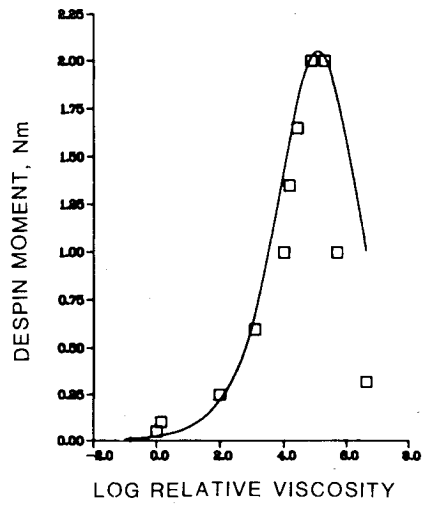

Fig. 1 Despin moment as a function of kinematic viscosity: squares denote data points and the solid line is the theoretical fit (see text).

log of the relative kinematic viscosity (with respect to that of water). The squares denote the data and the solid line is a curve of the form

$$\text{moment} = C_1 G/(C_2 + G)^2$$

where $G = \nu^{1/2}$ and C_1 and C_2 are constants to be determined from experiment. A dimensional picture was chosen because the relevant nondimensional number (E) one expects from the physics varies during an experiment. (If one were to base E on the initial rotation rate, the range corresponding to the experiment would be from 10^{-7} to unity.)

The curve shown has two arbitrary constants. They were chosen by requiring that the curve and the data match at the peak, and that the peak be at the viscosity shown. No other information from the data was used, so the correlation that appears must result from the form of the fit, which was chosen from the theoretical argument outlined earlier.

The reader will note that the agreement is poor at viscosities significantly higher than that at the peak. This is reasonable, since that at the peak corresponds to an E near 0.1, above which the boundary-layer approximation is likely to be poor. Thus it seems likely that the despin process, and by extension the flight data, reflects a resonance response to the coning motion, even at relatively high viscosities. (There is a large literature regarding flight instabilities at low viscosity. A comprehensive recent bibliography is given by Murphy.[5])

References

[1] D'Amico, W.P. and Miller, M.C., "Flight Instability Produced by a Rapidly Spinning Highly Viscous Liquid," *Journal of Spacecraft and Rockets*, Vol. 16, Jan.-Feb. 1979, pp. 62-64.

[2] Gans, R.F., "On the Precession of a Resonant Cylinder," *Journal of Fluid Mechanics*, Vol. 41, Pt. 4, 1970, pp. 865-872.

[3] Greenspan, H.P., *The Theory of Rotating Fluids*, Cambridge University Press, 1968, Chap. 1.

[4] Chandrasekhar, S., *Hydrodynamic and Hydromagnetic Stability*, Oxford University Press, 1961, Chap. 7.

[5] Murphy, C.H., "Angular Motion of a Spinning Projectile with a Viscous Liquid Payload," U.S. Army Ballistic Research Laboratory Rept. ARBRL-MR-03194, July 1982.

Three-Dimensional Wake Model for Low Earth Orbit

I. Katz,* D.L. Cooke,† D.E. Parks,‡ M.J. Mandell†
S-CUBED, La Jolla, California
and
A.G. Rubin§
Air Force Geophysics Laboratory, Hanscom Air Force Base, Massachusetts

Nomenclature

e	$= 1.6 \times 10^{-19}$ C
I	= ion current collected by a probe in wake
I_0	= ram ion current collected by a probe
n_i	= ambient ion density
V_{sat}	= satellite velocity
V_{th}	= ion thermal velocity
ϵ_0	= permittivity of free space
ϕ	= electrostatic potential
ρ	= charge density
θ	= electron temperature

Introduction

A CALCULATION of the electrostatic potential surrounding a model satellite which ignores ion focusing effects on space charge density is presented. The calculation is a three-dimensional simulation of a finite length right octagonal cylinder moving at Mach 8 through neutral plasma of ambient density $n_0 = 10^5$ cm^{-3} and temperature $\theta = 0.1$ eV. The object and the plasma parameters represent well the low-altitude AE-C satellite and its measured environment. Surface potentials on the object were obtained using the theory presented in Ref. 1. This yields a mean spacecraft potential in general agreement with that reported by Samir.[2] Wake ion densities were calculated assuming straight line trajectories, while electron densities were taken to be $n_0 \exp(e\phi/\theta)$, Ref. 3. The electrostatic potential ϕ was found by solving self-consistently Poisson's equation in the space around the object. Wake potentials and ion currents predicted by this model are compared with those obtained from AE-C data by Samir. Good agreement between observation and the predictions of this relatively simple theory is found.

Wake Potentials

Wake potentials are calculated using a preliminary version of POLAR, a computer code being developed to predict the charging of large space structures in three dimensions. The POLAR code presently consists of three major modules. The first is for object and mesh definition. The object definition is much along the lines of NASCAP[4] but more restrictive, there are no plans to include booms. The space around the object is broken up into discrete cells. Since the important regions are located along the flow direction, the mesh is staggered so that most of the cells are used to resolve wake and sheath phenomena.

Submitted March 4, 1983; revision received July 11, 1983.

*Program Manager.
†Research Scientist.
‡Senior Research Scientist.
§Staff Physicist.

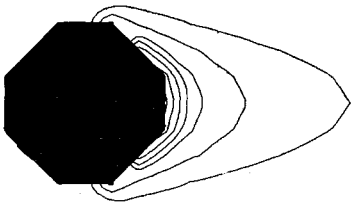

Fig. 1 Potential contours in the wake of the AE-C model; the outermost contour is −0.2 V, and the wake-side-pole potential is −1.5 V.

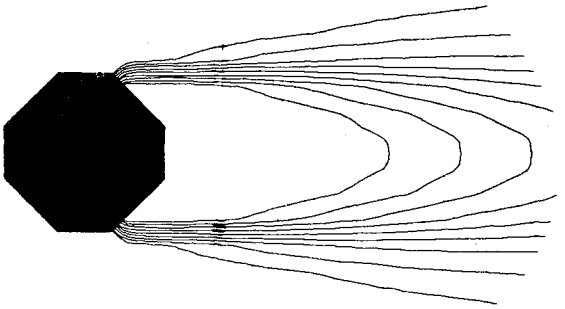

Fig. 2 Ion density contours in the wake of the AE-C spacecraft; the innermost contour represents one-tenth the ambient density, and the outermost 0.9 times ambient.

The second module calculates the "straight line approximation" density factors for the ions. This is done by calculating the shadowing of straight line orbits by the object. The straight line approximation to the density is particularly simple to calculate for two reasons. First, the straight line orbits allow trajectories to be "traced" instantly and, second, the orbits, and thus shadowing factors, are independent of particle kinetic energy. For every point in space the basic algorithm finds the perimeter of each object surface in solid angle space and eliminates all orbits within the perimeter from contributing to the local phase space density. While using only discrete directions this technique has proven extremely fast and quite accurate. The major approximations are the discretization of the angles and the interpolation in solid angle space of the surface perimeters. Typically, the solid angle space is gridded 36×180 and few extra points are added along each surface edge in order to minimize interpolation errors. The algorithm has been tested by comparing it with analytical results for densities near a surface. This straight line approximation to the ion density is only used for the charge formulation when solving for the space electric potential.

Sheath potential calculations are performed in the third module. The potentials are found by solving Poisson's equation

$$-\nabla^2\phi = \rho/\epsilon_0$$

where the approximations are all contained in the determination of the charge density ρ. We used a Boltzmann approximation for the electron density and the straight line ion density

$$\rho = -en_0 \exp(\phi/\theta) + en_i \text{ (straight line)}$$

Numerically, the nonlinear Poisson's equation is solved using the finite element approach previously employed in the NASCAP codes, although all the computer routines are new since the grid slicing algorithms force the computations to be performed in a very specific order.

Results

POLAR was used to calculate two models of the AE-C satellite in a low Earth environment represented by an O^+ plasma of density 10^5 cm^{-3} and temperature 0.1 eV. The Debye length for such a plasma is 0.74 cm. Since the AE-C is a cylinder, 114-cm long by 135-cm diameter, these models provide an excellent test of the high-density plasma charge density algorithm.

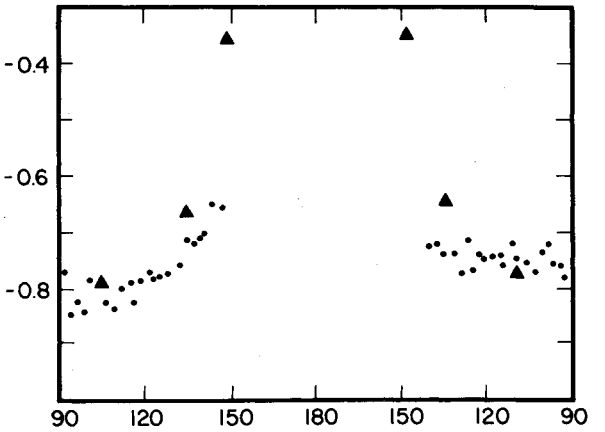

Fig. 3 Spacecraft potential (V) relative to plasma potential measured by rotating probe, plotted as a function of probe angle (deg). The points represents the data of Samir,[2] and the triangles represent the calculation of this work.

In both models, the satellite was modeled as a right octagonal cylinder of finite length. The first model has a rather coarse mesh spacing of 21.5 cm and was used to resolve much of the wake. The second model features a higher resolution spacing of 9.5 cm to allow predictions of the AE-C 30-cm probe potentials, but models less of the far wake. The models agree to within a few percent in the near wake and near surface potentials. Each calculation took about 20 min on a UNIVAC 1100/81.

Wake potential and ion density contour plots from the first calculation are shown in Figs. 1 and 2. These contours are in the planes bisecting the cylinder. The magnitude of the potential ranges from the −1.5 V, set on the wake-side pole surface based on Ref. 1, to zero in the undisturbed plasma. The potential varies most rapidly in the region directly behind the object. This region is not quasineutral; negative charge dominates, but the effective screening length is large. Thus no potential barrier is generated, although potential barriers are not excluded by the computational model (indeed, calculational examples showing barriers will be presented in Ref. 5). The formation of potential barriers requires surface potentials on the object much smaller in magnitude than the 15 times the electron temperature used in this calculation.

Calculated plasma potentials at a few locations along the path of the AE-C's guarded cylindrical electrostatic probe are compared with the results of Samir et al.[2] in Fig. 3. This comparison represents a good level (better than a factor of 2) of agreement between our theory and experiment.

An estimate of the ion current ratio I/I_0 can be obained using the relation

$$\frac{I}{I_0} \simeq \frac{n_i V_{\text{th}}}{n_i^0 V_{\text{sat}}}$$

This approximation should be reasonably accurate for deep wake ion currents away from the object when $V_{\text{sat}} \gg V_{\text{th}}$. A better treatment of probe currents would require, among other things, inclusion of cylindrical probe end effects, but neither our resolution nor the original experimental uncertainty would justify the effort. Using our model for the ion densities we determined $n_i/n_0 = 0.08$ for the probe location at 150 deg from the ram direction. With $V_{\text{th}}/V_{\text{sat}} = 0.13$, we estimated $I/I_0 = 0.01$. This is to be compared with the experimental value of 0.023. Considering the crudeness of the given current relation, this is a reasonable agreement.

Conclusions

The purpose of the calculations presented is to use existing flight data as a guide for the analytical model development program. Even though the primary aim of the POLAR program is to examine the possibility of substantial negative potentials occurring on large objects in polar orbit, the application of the code to the equatorial, nonsevere charging regime serves to examine the validity of the physical and comptuatioanl models. The results of these calculations showed a remarkably close correlation between theory and experiment. Nowhere was there as much as an order of magnitude disagreement in currents, or a factor of three in potentials. What was shown, instead, was reasonable agreement between theory and experiment. Much of the uncertainty could be traced to coarse geometrical modeling of the satellite and the straight line treatment of ion trajectories. Work is presently under way to include a more accurate representation of ion dynamics in the POLAR code. This work will be particulary important for more negative surface potentials than examined here, but will apply as well to the low Earth orbit near-wake problem.

Acknowledgments

This work supported by Air Force Geophysics Laboratory, Hanscom Air Force Base, Mass., under Contract F19628-82-C-0081.

References

[1]Parks, D.E. and Katz, I., "Mechanisms That Limit Potentials on Ionospheric Satellites," *Journal of Geophysical Research,* Vol. 88, A-11, Nov. 1983, pp. 9155-9162.

[2]Samir, U., Gordon, R., Brace, L., and Theis, R., "The Near-Wake Structure of the Atmosphere Explorer C (AE-C) Satellite: A Parametric Investigation," *Journal of Geophysical Reserach,* Vol. 84, A2, Feb. 1979, pp. 513-525.

[3]Laframboise, J.G. and Parker, L.W., "Probe Design for Orbit-Limited Current Collection," *Physics of Fluids,* Vol. 16, May 1973, pp. 629-636.

[4]Katz, I., Cassidy, J.J., Mandell, M.J., Schnuelle, G.W., Steen, P.G., and Roche, J.C., "The Capabilities of the NASA Charging Analyzer Program," *Spacecraft Charging Technology-1978,* NASA CP-2071, AFGL-TR-79-0082, 1979, p. 101.

[5]Cooke, D.L., Katz, I., Mandell, M.J., Parks, D.E., and Rubin, A.G., "Three-Dimensional Calculations of Barrier Formation in Satellite Wakes," presented at AGU Fall Meeting, San Francisco, Calif., Dec. 1982.

Design of a Minimum Acceleration Mortar Charge

G.R. Simpers* and K.P. Hall†
Naval Ordnance Station, Indian Head, Maryland

Introduction

LIGHTWEIGHT mortars are often used to deploy a variety of technical payloads. As a propulsion system they are generally inexpensive, reliable, and well suited to these types of payloads. The propulsive charge is commonly made up of flaked propellant with a large surface area per unit volume to minimize both the amount of propellant required and the effect of temperature on muzzle velocity. This approach results in high levels of acceleration of the payload. Some technical payloads are unable to withstand excessive acceleration levels. The "soft mortar charge" described in this Note minimizes the acceleration of the payload.

The key difference in the approach described is the use of uninhibited artillery propellant as the propulsive charge. This makes possible wide flexibility in the propulsion system design because artillery propellant grains are available in a variety of sizes.

Technical Approach

The goal of the mortar propulsion system described is the achievement of a certain muzzle velocity for a given payload and launcher system while limiting the maximum acceleration to between 300 and 500*g*. A conventional mortar propulsion unit previously used to launch a similar payload imparted an acceleration of 1200*g*. This level of maximum acceleration was too high for a new payload.

The mortar charge described is based on a "hi-lo" mortar concept. The propellant is burned in a high-pressure chamber and vented through nozzles into the closed breech volume behind the round. If the nozzles are properly sized, the ratio of chamber pressure to breech pressure can be kept high enough to ensure sonic flow in the nozzles. The pressure-time history in the propellant chamber is thereby divorced from the dynamics of the round in the launch tube.

The configuration of the mortar pressure chamber is shown in Fig. 1. Ignition is by means of the induction coil at the rear of the unit, which fires a squib into B/KNO_3 igniter pellets held in a hard case in the center of the chamber. Artillery propellant grains loosely surround the igniter in random array. The muzzle velocity achieved depends on the amount of propellant loaded, the surface area history of the individual grains, the nozzle area chosen, and the propellant characteristics.

The muzzle velocity of a mortar-launched round is established by the mission requirements of the payload. In order to achieve this velocity with minimum acceleration levels, the round should be accelerated at a constant rate throughout its travel down the launch tube. The ideal case of a constant acceleration means that the propellant grain must have a progressive surface area history. This is achieved in the present design by the use of uninhibited seven-perforation artillery grains. These grains are readily available in a number of granulations and propellant types. Our design used grains of M-30 propellant approximately 0.8 in. long.

The initial selection of web thickness for the propellant grain was made based on the desire to have the propellant burn out near the end of the launch tube. The geometry of an available grain with characteristics close to those desired was input into a computer program (SORN). This program calculates the internal ballistics of the propellant in the high-pressure chamber and the motion of the round when subjected to these forces.

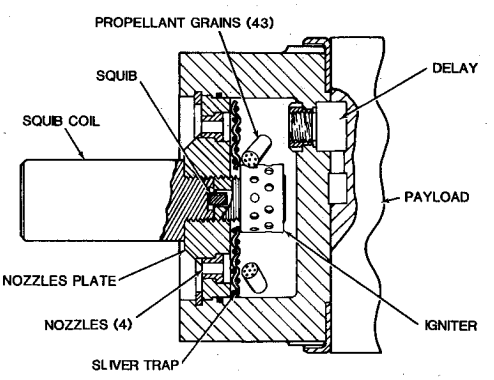

Fig. 1 Schematic of "soft" mortar charge using artillery propellant grains.

Presented as Paper 82-1147 at the AIAA/SAE/ASME 18th Joint Propulsion Conference, Cleveland, Ohio, June 21-23, 1982; received June 25, 1983; revision received Aug. 11, 1983. This paper is declared a work of the U.S. Government and therefore is in the public domain.

*Engineer. Member AIAA.
†Engineer. Associate Fellow AIAA.